Properties and DEFC tests of Nafion - Functionalized titanate nanotubes composite membranes prepared by melt-extrusion

B.R. Matos [a,*], C.A. Goulart [a], B. Tosco [b], J.S. da Silva [a], R.A. Isidoro [a], E.I. Santiago [a], M. Linardi [a], U. Schade [c], L. Puskar [c], F.C. Fonseca [a], A.C. Tavares [d]

[a] *Instituto de Pesquisas Energéticas e Nucleares, IPEN-CNEN/SP, São Paulo, 05508000, Brazil*
[b] *Universidade Federal Do ABC, UFABC, Santo André, SP, 09219170, Brazil*
[c] *Methoden der Materialentwicklung, Helmholtz-Zentrum für Materialien und Energie GmbH, Berlin, 12489, Germany*
[d] *Institut National de La Recherche Scientifique - Énergie, Matériaux et Télécommunications (INRS-EMT), 1650 Boulevard Lionel-Boulet, Varennes, Québec, Canada, J3X 1S2*

ARTICLE INFO

ABSTRACT

Nafion based composites are promising materials to improve the performance of direct ethanol fuel cells. In this work, composite membranes of Nafion and titanate nanotubes functionalized with sulfonic acid groups were prepared by melt-extrusion and tested in a direct ethanol fuel cell. Far and mid infrared spectroscopies evidenced the formation of ionic bridges between the sulfonic acid groups of both functionalized nanoparticles and the ionomer. Small angle X-ray scattering measurements revealed that the melt-extrusion method leads to an uniform distribution of the inorganic phase in the ionomer matrix. Such structural analysis indicated that the improved proton conduction properties of the composites, even with the addition of a high concentration of functionalized nanoparticles, are an outcome of the synergistic ionic network due to the hydrid organic/inorganic proton conducting phases. However, an improvement of the fuel cell performance is observed for 2.5 wt% of functionalized titanate nanotubes, which is a result of the lower ethanol crossover and the plasticizing effect of the aliphatic segments of the organic moieties grafted at the surface of the titanate nanoparticles.

1. Introduction

Composite electrolyte membranes based on the incorporation of an inorganic phase into ionomer matrices often show enhanced properties, such as high mechanical resistance and low permeability to solvents compared to the pristine ionomer membranes [1–5]. These properties are of paramount importance in direct alcohol fuel cells (DAFC), in which high mechanical resistance is required for reducing the plasticization of the solid electrolyte by the liquid fuel, and the low fuel crossover is necessary to minimize the depolarization of the cell [1,2]. However, one of the main drawbacks associated with composite membranes is the low proton conductivity of the electrolyte, since the nanoparticles are usually poor proton conductors. Another challenge, specific to DAFCs, is the poor proton conduction in alcoholic media [4].

The most commonly used nanoparticles are based on metal oxide materials such as SiO_2, TiO_2, ZrO_2, etc. [5–7]. Such particles possess high specific surface area and high hydrophilicity, but are characterized by a lower proton conductivity ($\sigma \sim 10^{-4}$ Scm^{-1}) compared to Nafion

($\sigma \sim 10^{-1}$ Scm^{-1}) [5]. In alternative, some efforts have been dedicated to the development of Nafion composite membranes containing proton conducting inorganic phases such as titanate nanotubes ($H_2Ti_3O_7.nH_2O$), zirconium phosphate ($Zr(HPO_4)$), and functionalized metal oxide nanoparticles [8–11]. It was reported that surface-functionalized titanate nanotubes display a proton conductivity of $\sigma \sim 10^{-2}$ Scm^{-1}, which is attractive for fuel cell applications.

Another important strategy is the addition of fiber-like nanoparticles into polymer matrices, which are known to enhance the water retention properties and the ion conductivity [4]. In addition, nanoparticles with a high aspect ratio increase substantially the mechanical properties of the polymer composites [9,12]. Furthermore, fiber-like mineral nanoparticles, in analogy with the titanate nanotubes, were shown to boost the proton conductivity by increasing the connectivity within the inorganic phase into the composite membranes [13].

The distribution of the nanoparticles in the ionomer matrix affects directly the direct ethanol fuel cell (DEFC) performance using the composites. For example, Nafion-Titanate nanotubes have been

---

* Corresponding author.
E-mail address: brmatos@usp.br (B.R. Matos).

prepared by casting and hydrothermal methodologies [9]. The former produces composite membranes with a poor distribution of the inorganic phase, whereas in the latter a fine dispersion of the nanotubes in the ionomer matrix is obtained. When uniformly dispersed in the matrix, the inorganic particles form an extended interface with the nanometric ionic domains of Nafion, leading to a higher connectivity of the ionic domains and creating new conduction pathways for proton migration [14]. In addition, a substantial enhancement of the mechanical properties and reduction of the alcohol crossover of the Nafion-Titanate prepared by hydrothermal method was observed compared to commercial Nafion membranes and to the Nafion-titanate prepared by casting.

Nonetheless, the casting methodology has the advantage of allowing the use of nanoparticles with distinct morphologies and functionalization prior to the fabrication of the composite solid electrolyte [9,14]. A preparation methodology that has been poorly explored for the preparation of composite ionomer membranes for fuel cells is the extrusion technique [15–18]. Twin melt-extrusion method consists of compounding mixtures of organic-inorganic phases in a broad range of compositions prior to passing matter through a orifice of well-defined shape. Twin extrusion offers a higher degree of dispersion of the nanoparticles within the polymer matrix, since both organic and inorganic phases are mixed at the melting point of the polymer by the extrusion screws [14,15]. The extrusion technique has attracted increasing importance for the preparation of electrolyte films for DAFC as being a cheaper production method of composite materials compared to traditional solution-casting [15]. Furthermore, the use of extrusion brings several beneficial aspects for the DAFC performance, for example: *i)* it also allows the use of particles of different morphologies and surface chemistries; *ii)* extruded materials display higher degree of crystallinity, which may increase the mechanical robustness of the film, and more importantly, lower methanol crossover [15–18].

Herein, composite membranes based on Nafion and titanate nanotubes functionalized with sulfonic acid groups were prepared by melt-extrusion. The composites were characterized by far and mid infrared spectroscopy (FIR and MIR), small angle X-ray scattering (SAXS), impedance spectroscopy (IS) and were tested in direct ethanol fuel cell. The new Nafion-titanate composites display a high degree dispersion of the inorganic phase within the ionomer matrix, and the functionalization of the titanate nanotubes resulted in a strong interaction between the nanoparticles and Nafion's ionic aggregates. Such features promoted an increase of the proton conductivity with increasing inorganic phase content and an improvement of the DEFC performance.

2. Experimental

2.1. Functionalization of the titanate nanotubes (TNTf)

The titanate nanotubes were prepared by an alkaline hydrothermal process by autoclaving a NaOH solution (10 mol L^{-1}) containing titania anatase nanoparticles (Degussa) at 110 °C for 24h, as described elsewhere [21]. The functionalization of the titanate nanotubes was performed by dispersing the titanate nanotubes in anhydrous toluene containing 3-mercaptopropyltrimetoxysilane (3-MPTMS/95% solution, Alfa Aesar) under continuous stirring. The grafting reaction was carried out under stirring at 60 °C for 6 h in a balloon bottle, and the MPTMS/TNT ratio varied from 10 to 60 wt%. The samples were filtered and washed with toluene twice and dried at 50 °C in vacuum for 2h. Details on the preparation and characterization of the titanate nanotubes can be found in previous publications [9–11].

The titanate nanotubes grafted with 3-MPTMS were used to prepare the Nafion composites, since the extrusion process is more difficult when the materials are in the ionic form because ionic crosslinks exist in the molten state [22]. Therefore, the oxidation of the silane moieties grafted at the titanate nanotubes surface to sulfonic acid groups (RSH → RSO$_3$H) was performed after the extrusion process along with the standard

cleaning and activation of the composite membrane.

2.2. Preparation of the Nafion – Functionalized titanate nanotubes composite membranes

The Nafion - functionalized titanate nanotubes (TNTf) composites were prepared by extrusion using a XPlore Conic Twin-Screw Micro-Compounder (~5 mL of capacity). The extruded composite cords were fabricated under co-rotation at 300 rpm and $T = 230$ °C, using mixtures of Nafion precursor (sulfonyl fluoride form/1100 gmol^{-1}, Ion Power®) and different concentrations of TNTf ranging from 0 to 15 wt% (ex. N-TNTf-0, N-TNTf-2.5, N-TNTf-5, N-TNTf-10 and N-TNTf-15). The segments of the extruded cords were hot-pressed at $T = 200$ °C (polymer only) and at $T = 230$ °C (composites) and a pressure of 200 kgfcm^{-2} for 2 min. Right after the hot-pressing, the films underwent quenching by immersing them for 2 min in liquid N$_2$ to suppress the samples' recrystallization. The presence of a high degree of crystallinity in Nafion was reported to reduce the degree of ionic conversion in the sample bulk with respect to the surface [23].

At this stage, both the polymer and the grafted titanate nanotubes must undergo the conversion of their functional groups into the sulfonic acid form. First, the SO$_2$F groups of Nafion were converted into SO$_3$Na. This reaction was carried out by placing the Nafion and the composite films in a water/DMSO/NaOH solution (50/35/15 vol%) for 6 h at 80 °C. The membranes were cleaned 3 times with deionized water for 1 h at 80 °C. Next, the mercapto groups of the titanate nanotubes were oxidized to SO$_3$H groups by placing the composite membranes in a H$_2$O$_2$ (3 vol%) solution for 1 h at 80 °C. The acidification of Nafion composites was performed in three steps: two treatments in HCl solution (0.1 molL^{-1}) and one last one at H$_2$SO$_4$ (0.5 molL^{-1}) at 80 °C for 1 h. All these steps were intermediated by washing with deionized water at 80 °C for 1 h to remove the excess of chemicals.

2.3. Physicochemical characterization of the functionalized nanotubes and composite membranes

The morphology of the titanate nanotubes was studied by field-emission scanning electron microscopy (FE-SEM, JEOL model JSM-6701F). Transmission electron microscopy (TEM) images of the titanate nanotubes were recorded using a JEOL-2100F instrument with 200 kV of applied voltage.

The CHNS analysis, also known as dynamic flash combustion method, was carried out on the functionalized samples in order to quantify the amount of grafted silane from the percentage of S. CHNS elemental analyses of the functionalized nanotubes were performed in the Elemental Analysis Laboratory of the University of Montreal, using an analyzer EAS1108, Fisons Instruments S.p.A. Specifically, the sample (~2 mg) is weighed and put in a tin capsule, and introduced in to a quartz tube reactor under a flow of He enriched with O$_2$. The sample and the tin capsule react with oxygen at 1700–1800 °C, and are broken into their elemental components, N$_2$, CO$_2$, H$_2$O and SO$_2$. The gas composition is analysed by a thermal conductivity detector, and a signal proportional to the amount of each element in the sample is generated. The elemental peaks are compared to a known standard and the elemental wt% quantified. The accuracy of the results is ±5% for each element.

N$_2$ sorption isotherms of the functionalized titanate nanotubes were measured at −196 °C down to relative pressure P/Po 5x10^{-7} with Quantachrome Instrument Autosorb. The samples were weighed and placed on the analysis port. Before the sorption measurement, each sample was heated at 60 °C for 2h under vacuum. The specific surface area was obtained by the BET method, while the micropore and the mesopores volumes were determined by applying the *t*-plot de Boer and the BJH methods, respectively. The sorption data were analysed using Autosorb Software from Quantachrome Instrument.

The equivalent weight (*EW*) of the composite membranes was determined by acid-base titration using the relation $EW = m/M\,v$; where

m is the dry mass of the composite recorded after acidification treatment; M is the solution molarity; and v is the titrated volume. The membranes in the H$^+$ form were placed in a 1 M NaCl solution for 30 min and the proton concentration back titrated with a 0.01 M NaOH solution, standardized with potassium biphtalate. The water uptake (WU) was obtained as the ratio between the mass of the absorbed water by the mass of dry polymer.

Mid infrared (MIR) Fourier Transform (FT) spectroscopy measurements were performed with a Nicolet 6700 spectrometer in the attenuated total reflectance (ATR) mode using a ZnSe crystal. Each spectrum is an average of a total of 96 scans with a spectral resolution of 4 cm^{-1} in the 4000 to 600 cm^{-1} range at room T (25 °C) and RH (40%). For these measurements, the composite samples were previously dried in a vacuum oven for 1 h at room T and immediately placed at the spectrometer to avoid extensive absorption of water from the environment.

Far infrared (FIR) and MIR FT spectra were also measured at the IRIS beamline at the electron storage ring BESSY II of Helmholtz Zentrum Berlin [24]. The measurements for both FIR and MIR were done in transmission mode in vacuum (<0.1 mbar) in the sample compartment of a Bruker Vertex 70/v spectrometer. FIR spectra in spectral region between 600 and 30 cm^{-1} were measured with 2 cm^{-1} resolution using infrared synchrotron radiation as a source together with a liquid helium cooled silicon bolometer and a silicon beamsplitter. For these measurements 128 scans were co-added. For the MIR transmission measurements the internal globar source was employed together with a DLaTGS detector and a KBr beamsplitter. The spectra were taken at 4 cm^{-1} resolution and 32 scans were co-added. For both the spectral regions investigated, references were taken through the empty channel inside the spectrometer sample compartment under vacuum. The data acquisition started when no more changes in the water related features were observed spectroscopically.

SAXS experiments were carried out using synchrotron radiation at the SAXS beamline of the Brazilian National Synchrotron Light Laboratory (LNLS). The experiments were conducted with an incident wavelength $\lambda = 1.488$ Å in the range of the scattering vector $q \sim 0.02$–0.35 Å^{-1} ($q = 4\pi \sin \theta/\lambda$, with 2θ being the scattering angle). Scattering patterns were collected with MarCCD detector and the intensity curves corrected for parasitic scattering, integral intensity, and sample absorption.

Impedance spectroscopy (IS) data were collected in an especially designed air-tight sample holder able to measure the proton conductivity in the range $T = 30$–200 °C with $RH = 100\%$ [19]. A Solartron 1260 frequency response analyzer was used for IS measurements in 4 mHz–3 MHz frequency (f) range with 100 mV ac amplitude. The resistance of the samples was obtained from the intercept of the impedance semicircle at high frequencies ($f \sim 10^6$ Hz) with the real axis of the complex plane [25]. In order to compare the proton conductivity with the sample water content, the high frequency range of the conductivity was used, which is associated with the short-range displacements of the proton in aqueous media [25]. The low frequency study of the proton conductivity, i.e., the dc proton conductivity will be devoted to a further study. The measurements were performed in triplicates, and the associate experimental error is 10%.

Differential scanning calorimetry (DSC) was performed on dry Nafion with DSC Q200 – TA instruments under nitrogen flow in two successive heating scans from −50 to 250 °C at a heating rate of 20 °C min^{-1} under nitrogen flow. A fast cooling step (50 °C min^{-1}) was used between the heating steps. The thermal event observed in the first heating associated with the order-disorder transition of the sulfonic groups is absent in the second heating (not shown), following the typical behavior observed for Nafion [31].

2.4. Direct ethanol fuel cell tests

Extruded Nafion and the composite membranes were evaluated in 5 cm^2 single fuel cells. MEAs were fabricated by hot pressing both electrodes to the fabricated membranes at 125 °C and 1000 kgf cm^{-2} for 2 min. The anode catalyst layer was composed of 1.0 mg cm^{-2} PtSn/C (Pt:Sn of 75:25 Etek) and 30 wt% of dry Nafion (Dupont). The cathode catalyst layer contained 1.0 mg cm^{-2} Pt/C (20%, Etek) and 30 wt% Nafion. The thicknesses of the hydrated membranes were ~160 μm. The single cell was fed at the anode with 1.0 mol L^{-1} ethanol solution and 5.0 mL min^{-1} flux at 1 atm, and at the cathode with pure oxygen at 3 atm absolute pressure. Fuel cell and oxygen humidifier temperatures were varied from 80 °C to 110 °C and polarization curves were obtained in duplicate experiments with estimated error of ~10% between 80 °C and 110 °C. For each measuring temperature, after temperature stabilization the system was conditioned by draining electrical current at a fixed voltage of 0.7 V for 2 h before data collection in order to reach steady state.

3. Results and discussion

Fig. 1a shows the SEM images of the titanate nanotubes, and the corresponding high magnification image obtained by TEM is shown in Fig. 1b.

The images of the titanate nanotubes show a distribution of a relatively large volume fraction of nanoparticles with an average diameter of ~10 nm and length of ~100 nm, in good agreement with reported typical nanotube dimensions [9,21]. The titanate nanotubes consist typically of 3–5 multiple layers tubes with internal and external diameters ranging between 3-5 and 7–10 nm, respectively, and characteristic length of hundreds of nanometers (100–300 nm) [9,21]. Fig. 1b evidences the tubular nanostructures with characteristic dimensions compatible to the ones usually reported for titanate nanotubes in the powder form, confirming the exit in the preparation of the inorganic phase.

Fig. 2a shows the variation of sulfur content in the modified titanate nanotubes with the MPTMS/TNT ratio before and after the oxidation of the thiol groups. Prior to the silane oxidation, the sulfur content on the titanate nanotubes increases with the MPTMS concentration in the grafting solution. A plateau is nevertheless observed for MPTMS/TNT ratio >40 suggesting that at high silane concentration, a fully coverage of the surface of the titanate nanotubes takes place [26]. Such hypothesis is confirmed by the ratio S/C which increases with increasing MPTMS/TNT in a similar trend. In contrast, after the conversion of the thiol groups into sulfonic acid groups, the amount of sulfur is fairly constant among all samples. However, the S/C ratio decreases with increasing MPTMS/TNT ratio in the entire range investigated. Such trends indicate that the self-polymerization of the mercapto – precursor competed with the grafting reaction on the surface of the nanotubes, and that the non-grafted MPTMS is washed away during the washing and oxidation steps [3,26].

In Fig. 2b it is shown that the specific surface area of the nanotubes decreases from 340 m^{2}g^{-1} for the non-modified TNT to 240 m^{2}g^{-1} (40 wt %), which is consistent with an increase of the extent of grafting, and possibly a reduced porosity of the grafted nanotube surface [3,26]. Considering both the sulfur content and the specific surface area of the functionalized nanotubes, nanotubes obtained from 40 wt% MPTMS/TNT were chosen for preparing the composite samples.

FTIR spectroscopy was used to investigate the conversion of the Nafion precursor into its ionic form, and of the –SH into SO$_3$H groups in the composite membranes. Representative spectra are shown in Fig. 3. The spectrum of Nafions' non-ionic form contains a band at 1470 cm^{-2} assigned to the SO$_2$ stretching in SO$_2$F [27]. After the conversion, the typical vibrational bands of Nafion can be observed in the FTIR spectra (Fig. 3a and b). The band at 1060 cm^{-1} is assigned to the symmetric S–O stretching vibrations from the SO$_3^-$ groups. The bands at 1220 and 1150 cm^{-1} are attributed to the symmetric and asymmetric stretching of CF$_2$, respectively. And the bands at 980 and 960 cm^{-1} are assigned to the symmetric vibrations from two C–O–C linkages residing in two distinct chemical environments [22,24,28].
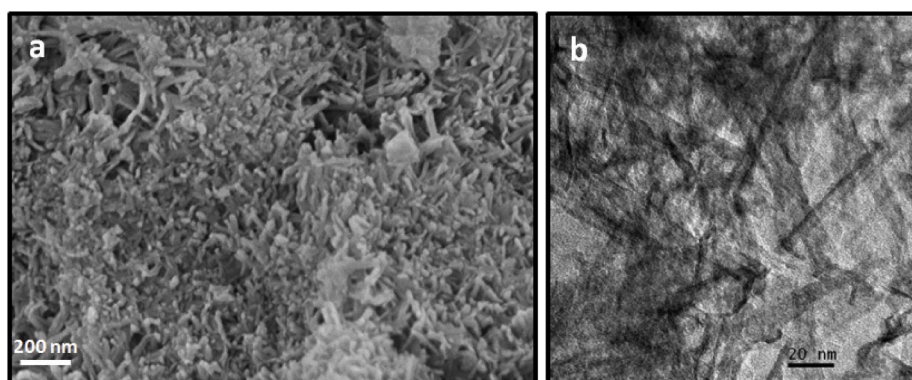
Fig. 1. SEM (a) and TEM (b) images of the titanate nanotubes in the proton form.
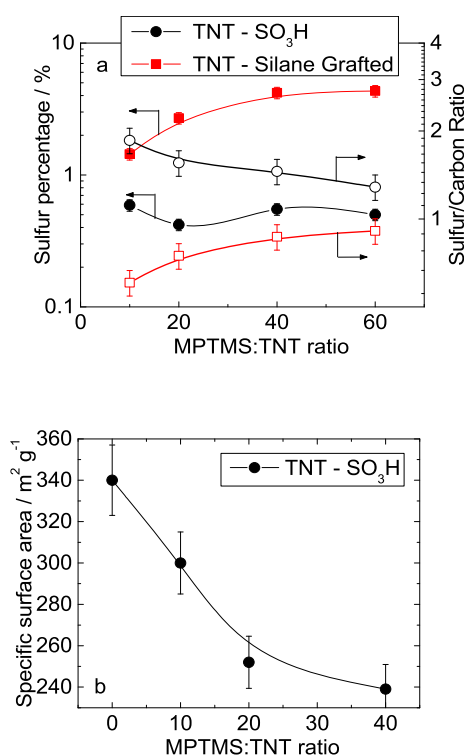

Fig. 2. (a) Sulfur content of the modified titanate nanotubes (left axis) and sulfur/carbon percentage ratio (right axis) with the 3-MPTMS/TNT ratio, before and after the oxidation of the thiol groups. (b) Specific surface area of the grafted titanate nanotubes with the 3-MPTMS/TNT ratio.

Fig. 3. FTIR-ATR spectra of (a) Nafion precursor (SO_2F form) and converted into the SO_3H from; and (b) melt-extruded Nafion (N-TNT-0) and composite Nafion-titanate nanotubes (N-TNTf-15) membranes.

In Fig. 3b, the spectrum of Nafion containing functionalized titanate nanotubes (N-TNTf-15) displays additional peaks at 2918 and 2844 cm^{-1}, assigned to the grafted C–H moieties in the inorganic phase [29,30]. The transmittance spectrum of N-TNTf-15 displays no noticeable band in the 2550–2620 cm^{-1} range, which is consistent with the conversion of the anchored thiol groups [29,30]. The conversion of the thiol groups originating from the sulfonyl fluoride matrix and from the anchored thiol groups can also be attested by ion exchange capacity measurements. According to these measurements, the functionalization of the titanate nanotubes contributed the ion exchange capacity of the composites, which increased with the content of the inorganic phase: N-TNTf-2.5 (~0.92 $mEqg^{-1}$), N-TNTf-5 (~0.95 $mEqg^{-1}$), N-TNTf-10 (~1.00 $mEqg^{-1}$), N-TNTf-15 (~1.07 $mEqg^{-1}$). These values are very close to the expected value of ion exchange capacity (~0.90 $mEqg^{-1}$). The water uptake of the all composites is nearly constant (30 wt%), but is higher than that of the melt-extruded Nafion
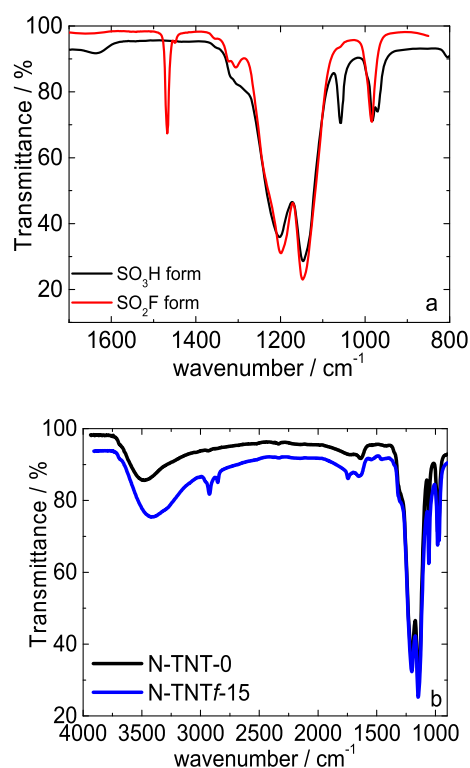
membrane (NTNTf-0, 24 wt%) in excellent agreement with the higher amount of acidic groups in the composites.

Evidence the cation motion of the translational motion of protons along the ionic clusters in Nafion can be given by Far infrared measurements [22,24]. Yet, to first characterize the state of aggregation of the sulfonic acid groups in the functionalized TNTs, Nafion sulfonyl fluoride composites were treated with H_2O_2 and H_2SO_4 only. As expected, the FIR spectrum of pristine polymer films that underwent such treatment displays only the characteristic bands of the nonionic form [22]. Fig. 4a and b show in addition the far (500–20 cm^{-1}) and mid infrared spectra (4000–1250 cm^{-1}) respectively, of N-TNTf in the SO_2F form.

The spectrum of N-TNTf (SO_2F) differs from that of Nafion-SO_2F by the presence of a broad band in the 350–50 cm^{-1} range, peaking at ~ 250 cm^{-1}. This band is clearly identified in the N-TNTf-15 spectrum, and is attributed to a convolution of bands associated with the cation motion within SO_3H clusters (240 cm^{-1}) and the typical bands of
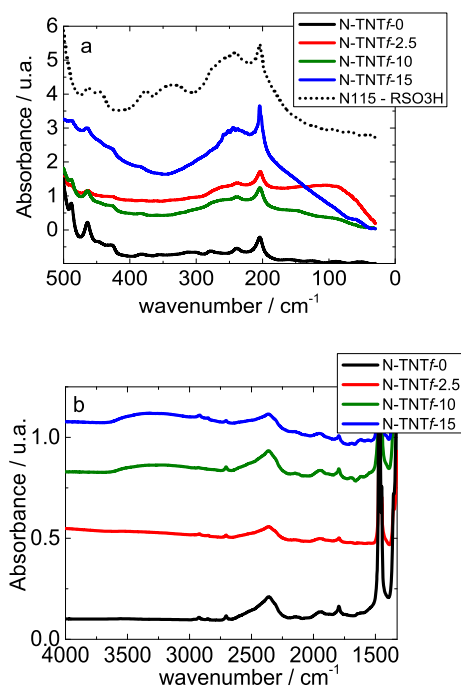
Fig. 4. **(a)** Far (500–20 cm^{-1}) and **(b)** mid (4000–1300 cm^{-1}) infrared spectra recorded under vacuum and in the transmission mode of composite films formed by N-TNT*f* and Nafion in the SO$_2$F. The spectra of Nafion in the ionic and non-ionic forms are shown for comparison.

Ti–O vibrations in titanate nanotubes lattice (181 and 270 cm^{-1}). Nafion's typical CF$_2$ rocking band is seen at 204 cm^{-1}. The spectrum of Nafion in the proton form also shows three bands at ∼ 240, 335, and 375 cm^{-1} which are assigned to H-bond stretching involving the hydronium ion in RSO$_3$H [22,24]. Since the FTIR measurements were performed under vacuum, the water sorption by these samples is negligible, resulting in the absence of the 335 and 375 cm^{-1} bands (Fig. 4a). The band associated with the hydrogen bonding within SO$_3$H groups (3200 cm^{-1}) is present in the spectra of the composites with concentrations of the inorganic phase above > 2.5 wt%, Fig. 4b. The observed OH stretching band may be due to the hydrogen bonding among titanate nanotube particles and among sulfonic acid groups. It is important to stress that the presence of ionic clusters in the nanoparticles can help improving the connectivity of the conduction pathway for proton transport in the ionomer matrix.

SAXS measurements were performed to evaluate the distribution of the nanoparticles in the Nafion matrix. Fig. 5a displays a comparison of the SAXS patterns of the N-TNT composites in the SO$_3$H form prepared
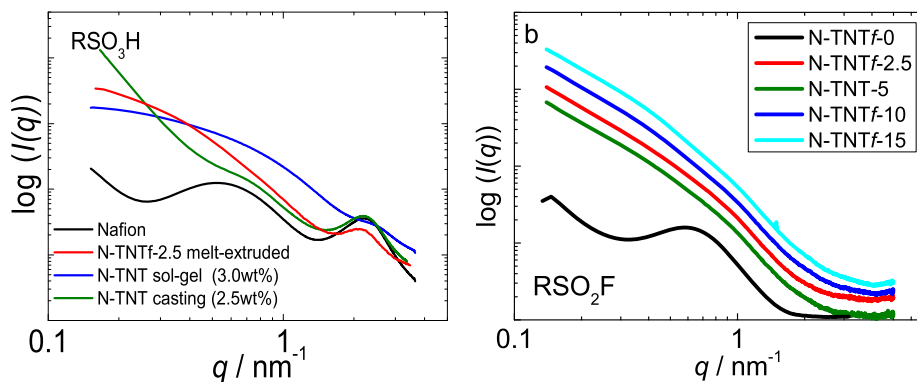
by different methods: casting, sol-gel and extrusion (N-TNT*f*-2.5). Fig. 5b shows the SAXS patterns of N-TNT*f* composites and of Nafion in the SO$_2$F form.

As illustrated in the figure, Nafion's SAXS pattern displays the matrix peak at q ∼0.6 nm^{-1} and the ionomer peak at q ∼2 nm^{-1} [23]. Instead, the SAXS plots of the composites display only the ionomer peak, because the matrix peak is superposed with the X-ray scattering from the nanoparticles at $q < 2$ nm^{-1}. The differences between the scattering patterns of the composites at low q are the result of difference in the distribution of the inorganic phase in the ionomer matrix. The casting method produces composite membranes with a poor distribution of the titanate nanotubes, as indicated by the upturn in scattering intensity at $q < 0.6$ nm^{-1}, which is mostly due to the correlation length among the nanoparticles, and indicates a higher degree of aggregation of nanoparticles of the composites prepared by casting [20]. On the other hand, the SAXS curves of Nafion-titanate samples prepared by sol-gel and melt-extrusion exhibit scattering patterns forming a plateau for $q < 0.3$ nm^{-1}, which suggests that such scattering is associated with the shape of the nanoparticles, and an absence of interparticle correlation. This feature indicates a low degree of aggregation among the nanoparticles. Still, the SAXS measurements of the N-TNT*f* in the nonionic form (Fig. 5b) display a linear dependence for $q < 0.3$ nm^{-1} indicating some agglomeration of nanoparticles. The differences between the SAXS curves at low q ($q < 0.3$ nm^{-1}) for N-TNT in the nonionic and ionic forms (Fig. 5a and b) may be also due to scattering differences in the ionomer matrix due to ionic conversion [22]. However, compared with the composites prepared by casting, the melt-extruded composites do not exhibit an increase of the particle aggregation with increasing the inorganic phase content, as shown in Fig. 5b. Such feature evidences the ability of preparing composites with a wide range of composition displaying a high degree of homogeneity.

Fig. 6 shows the Arrhenius plots for the proton conductivity of Nafion and the N-TNT*f* composites. The Arrhenius plots were built using the proton conductivity values obtained from the high frequency intercept in the impedance spectra (Z" → 0 at f ∼ 10^6 Hz) of fully hydrated membranes. It was previously shown that at such frequency range, the motion of protons corresponds to forward-backward fluctuations of high mobility protons across a nanometer length-scale (∼10^{-1} to 10^1 nm) in hydrated domains of Nafion [25].

The proton conductivity of the composites is lower than the one observed for melt - extruded Nafion. The lower conductivity of the composites with respect to the pristine Nafion is probably due to the lower proton conductivity of functionalized titanate nanotubes (10^{-2} Scm^{-1}) [21]. Still, an important aspect of the N-TNT*f* composites, and not found in the ones prepared by the other methods [9–11], is the higher proton conductivity of N-TNT*f*-15 compared to that of the composites with lower fractions of TNT*f*. In addition, the drop of conductivity is much smaller in the N-TNT*f* composites compared to the those

Fig. 5. Comparison of SAXS patterns from **(a)** N-TNT composites in the SO$_3$H form prepared by different methods: casting, sol-gel and extrusion (N-TNT*f*-2.5); **(b)** melt-extruded composites in the sulfonyl fluoride form with different amounts of functionalized titanate nanotubes.
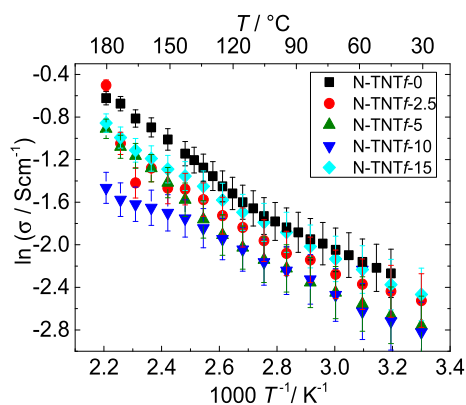
Fig. 6. Arrhenius plots for the proton conductivity of Nafion and the N-TNT*f* composites. Impedance spectroscopy measurements were done at 100% RH.

usually observed for composite membranes prepared with titania or silica nanoparticles [5,9,29].

Nafion displays an upturn of the proton conductivity for $T > 90$ °C, which is due to a crossover from the Arrhenius-like to the Vogel-Tamman-Fulcher (VFT) temperature dependence of the proton conductivity [19]. Such upturn is not observed in the composite samples. In fact, the proton conductivity for the composites at $T > 90$ °C does not follow the VTF behavior which has been related to the modulation of the proton transport by thermally activated correlated motion of the main and side chains. The different conductivity – temperature behavior of the composite membranes is an evidence that the hydrocarbon grafted chains are contributing to the proton transport in the sample. Such feature is in good agreement with the FTIR data and may be the reason for the higher proton conductivity for the composites with high concentration of nanoparticles (N-TNT*f*-15). Specifically, the addition of grafted titanate nanotubes improves the phase separation into the ionic and nonionic domains, increasing the mean free path for proton migration. Moreover, according to the Vogel-Tamman-Fulcher empirical law, the nonlinear increase of the proton conductivity with increasing T is associated with a temperature dependent reduction of the viscosity of the medium for glass-like materials [32]. In polymer systems, such phenomenon is associated with a cooperative motion between the proton transport and the mobility of the main and side chains. The higher flexibility of the polymer chains due to the plasticizing effect of the grafted moieties may contribute positively to the proton conductivity of the composite membranes.

Fig. 7 shows that the DEFC performance of the N-TNT*f*-2.5 composite is higher than that of Nafion. The addition of a small amount of functionalized nanoparticles into Nafion, resulting in composite membranes with higher water sorption capacity and higher proton conductivity compared to composite membranes prepared from non-functionalized
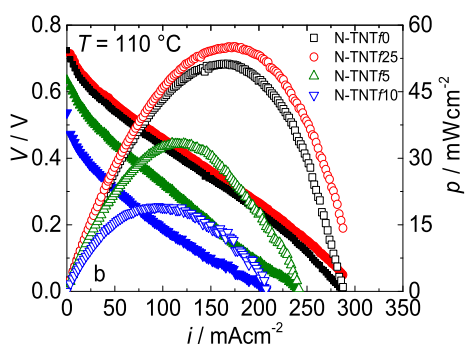
ones, is indeed a promising strategy to improve the fuel cell efficiency. However, the performances of composites with higher content of nanoparticles are significantly lower. In particular, the DEFCs show a lower open circuit voltage, which is usually associated with a high fuel crossover across the membrane. Besides, no substantial changes of the slope in the ohmic region of the polarization curve are observed, in good agreement with the proton conductivity measurements.

In fact, the N-TNT*f* composites exhibit higher macroscopic flexibility than the composites prepared with non-functionalized nanoparticles. As a result, composites with high nanoparticles content could not be tested at T above 130 °C due to the formation of pinholes, pointing for a low thermomechanical property of these films. In order to evaluate the thermal behavior of the composite membranes, DSC measurements were carried out and the results are shown in Fig. 8.

The DSC scan of N115 displays an endothermic minimum centered at 145 °C, which is characterized as the relaxation of the hydrogen bonding among sulfonic acid groups, usually termed as α-transition [33]. The DSC scans of the composite membranes exhibit a marked shift of such minimum from 145 to 97 °C for N-TNT*f*-2.5 indicating that the addition of TNT functionalized with sulfonic groups contributed to the weakening of the electrostatic interactions among sulfonic groups into the composite. However, with increasing of the fraction of TNT*f* from 2.5 to 15%, the endothermic minima shifted from 97 to 112 °C and a second endothermic peak appears around 150 °C for TNT*f* $\geq$ 10 wt%. These results suggest that higher loadings of the TNT*f* may bring beneficial effects to the thermomechanical properties of the Nafion- TNT*f* composites. It has been previously reported that the neutralization of Nafion with alkylammonium counterions with different lengths of the hydrophobic moieties promoted a plasticization of the hydrophobic parts of Nafion chains and reduced significantly (~50 °C) the α-transition temperature [28,31]. The DSC results raise a question on the effect of the length of the C–H moieties of the TNT*f* on the mechanical and electrical properties of functionalized composites. Possibly, the self-polymerization of the silane precursor results in longer hydrocarbon chains that will favor interactions between the functionalized nanoparticles and the hydrophobic domains of Nafion. Since the ethanol molecules display affinity for both hydrophilic and hydrophobic phases of Nafion, the existence of higher fractions of flexible hydrophobic phase and higher water uptake into Nafion-Titanate composites may contribute to the increase of the permeability to ethanol in the membranes. Such investigation is a topic of further communication and is out of the scope of this work.

4. Conclusions

The use of melt-extrusion technique allowed producing composite membranes of Nafion-titanate nanotubes aggregating several important synergistic features that are known to maximize the proton conductivity. The extrusion method used permitted preparing Nafion with addition of

Fig. 7. DEFC polarization curves and power densities recorded obtained at 110 °C with the composite electrolytes. The fuel cell is fed with 1 M ethanol solution at 5 mL min^{-1} rate (1atm) at the anode and with O_2 at 3 atm at the cathode.
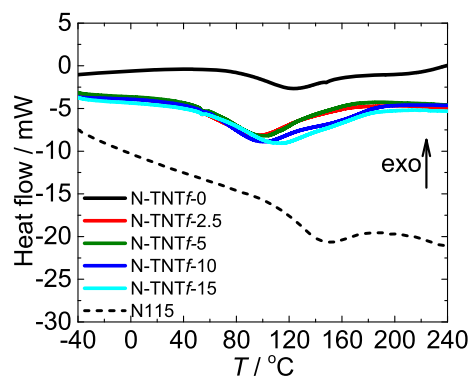

Fig. 8. DSC scans of the melt-extruded N-TNT*f* composite membranes.

high surface specific area and acid sulfonic functionalized titanate nanotubes with a higher degree of distribution of the inorganic phase into the ionomer matrix, even for high-load composites as revealed by SAXS. Moreover, FIR measurements allowed discerning that the additional ionic groups contained in the inorganic phase are interacting with the ionic domains of Nafion. The intimate supramolecular interactions of the organic and inorganic phases contributed to increase the composite water content and, more importantly, to increase the proton conductivity with increasing inorganic phase. The DEFC performance was improved for composites with 2.5 wt% titanate nanotubes content, indicating that melt-extruded composites are promising materials for DEFC electrolytes.

Declaration of competing interest

The authors declare that they have no known competing financial interests or personal relationships that could have appeared to influence the work reported in this paper.

CRediT authorship contribution statement

B.R. Matos: Conceptualization, Methodology, Formal analysis, Writing - review & editing. **C.A. Goulart:** Formal analysis. **B. Tosco:** Formal analysis. **J.S. da Silva:** Formal analysis. **R.A. Isidoro:** Formal analysis. **E.I. Santiago:** Formal analysis. **M. Linardi:** Formal analysis. **U. Schade:** Formal analysis. **L. Puskar:** Formal analysis, Writing - review & editing. **F.C. Fonseca:** Formal analysis, Writing - review & editing. **A.C. Tavares:** Supervision, Conceptualization, Methodology, Formal analysis, Writing - review & editing.

Acknowledgements

References

[1] X. Li, E.P.L. Roberts, S.M. Holmes, Evaluation of composite membranes for direct methanol fuel cells, J. Power Sources 154 (2006) 115–123.

[2] S. Song, P. Tsiakaras, Recent progress in direct ethanol proton exchange membrane fuel cells (DE-PEMFCs), Appl. Catal. B Environ. 63 (2006) 187–193.

[3] B. Mecheri, V. Felice, Z. Zhang, A. D'Epifanio, S. Licoccia, A.C. Tavares, DSC and DVS investigation of water mobility in Nafion/Zeolite composite membranes for fuel cell Applications, J. Phys. Chem. C 116 (2012) 20820.

[4] Z. Zhang, F. Désilets, V. Felice, B. Mecheri, S. Licoccia, A.C. Tavares, On the proton conductivity of Nafion–Faujasite composite membranes for low temperature direct methanol fuel cells, J. Power Sources 196 (2011) 9176–9187.

[5] B.R. Matos, R.A. Isidoro, E.I. Santiago, F.C. Fonseca, Performance enhancement of direct ethanol fuel cell using Nafion composites with high volume fraction of titania, J. Power Sources 268 (2014) 706–711.

[6] D. Cozzi, C. de Bonis, A. D'Epifanio, B. Mecheri, A.C. Tavares, S. Licoccia, Organically functionalized titanium oxide/Nafion composite proton exchange membranes for fuel cells applications, J. Power Sources 248 (2014) 1127–1132.

[7] B. Mecheri, V. Felice, A. D'Epifanio, S. Licoccia, A.C. Tavares, Composite polymer electrolytes for fuel cell applications: filler-induced effect on water sorption and transport properties, ChemPhysChem 14 (2013) 3814–3821.

[8] D. Truffier-Boutry, A. De Geyer, L. Guetaz, O. Diat, G. Gebel, Structural study of zirconium Phosphate–Nafion hybrid membranes for high-temperature proton exchange membrane fuel cell applications, Macromolecules 40 (2007) 8259.

[9] B.R. Matos, R.A. Isidoro, E.I. Santiago, M. Linardi, A.S. Ferlauto, A.C. Tavares, F. C. Fonseca, In situ fabrication of nafion–titanate hybrid electrolytes for high-temperature direct ethanol fuel cell, J. Phys. Chem. C 117 (2013) 16863–16870.

[10] B.R. Matos, E.I. Santiago, J.F.Q. Rey, A.S. Ferlauto, E. Traversa, M. Linardi, F. C. Fonseca, Nafion-based composite electrolytes for proton exchange membrane fuel cells operating above 120 C with titania nanoparticles and nanotubes as fillers, J. Power Sources 196 (2011) 1061–1068.

[11] B.R. Matos, E.I. Santiago, F.C. Fonseca, M. Linardi, V. Lavayen, R.G. Lacerda, L. O. Ladeira, A.S. Ferlauto, Nafion–titanate nanotube composite membranes for PEMFC operating at high temperature, J. Electrochem. Soc. 154 (2007) B1358–B1361.

[12] F. Xu, S. Mu, M. Pan, Decoration of carbon nanotube with SiO₂ nanoparticles to improve polyelectrolyte membrane performance, J. Nanosci. Nanotechnol. 11 (2011) 10896–10899.

[13] F. Xu, S. Mu, M. Pan, Mineral nanofibre reinforced composite polymer electrolyte membranes with enhanced water retention capability in PEM fuel cells, J. Med. Sci. 377 (2011) 134–140.

[14] G. Alberti, M. Casciola, Composite membranes for medium-temperature PEM fuel cells, Annu. Rev. Mater. Res. 33 (2003), 29-154.

[15] Y. Treekamol, M. Schieda, L. Robitaille, S.M. MacKinnon, A. Mokrini, Z. Shi, S. Holdcroft, K. Schulte, S.P. Nunes, Nafion®/ODF-silica composite membranes for medium temperature proton exchange membrane fuel cells, J. Power Sources 246 (2014) 950–959.

[16] A. Mokrini, N. Raymond, K. Theberge, L. Robitaille, C. Del Rio, M.C. Ojeda, P. G. Escribano, J.L. Acosta, Properties of melt-extruded vs. solution-cast proton exchange membranes based on PFSA nanocomposites, ECS Trans. 33 (2010) 855–865.

[17] A. Mokrini, A. Siu, L. Robitaille, L. Gonzalez, F. Sanchez, Investigation of advanced hybrid PEM based on sulfonyl fluoride PFSA and grafted inorganic nanoparticles, ECS Trans. 33 (2010) 823–838.

[18] A. Mokrini, M.A. Huneault, Z. Shi, Z. Xie, S. Holdcroft, Non-fluorinated proton-exchange membranes based on melt extruded SEBS/HDPE blends, J. Membr. Sci. 325 (2008) 749–757.

[19] B.R. Matos, C.A. Goulart, E.I. Santiago, R. Muccillo, F.C. Fonseca, Proton conductivity of perfluorosulfonate ionomers at high temperature and high relative humidity, Appl. Phys. Lett. 104 (2014), 091904.

[20] J.E. Mark, in: J.E. Mark, C. Y-C Lee, P.A. Bianconi (Eds.), Hybrid Organic-Inorganic Composites, ACS Symposium Series, 585, American Chemical Society, Washington, DC, 1995. Ch 1.

[21] D.V. Bavykin, J.M. Friedrich, F.C. Walsh, Protonated titanates and TiO₂ nanostructured materials: synthesis, properties, and applications, Adv. Mater. 18 (2006) 2807–2824.

[22] B.R. Matos, R. Politano, J.F.Q. Rey, D. Hermida-Merino, U. Schade, L. Puskar, F. C. Fonseca, Interplay of α/β-Relaxation dynamics and the shape of ionomer building blocks, Sci. Rep. 8 (2018) 13441.

[23] M.-H. Kim, C.J. Glinka, S.A. Grot, W.G. Grot, SANS study of the effects of water vapor sorption on the nanoscale structure of perfluorinated sulfonic acid (NAFION) membranes, Macromolecules 39 (2006) 4775–4787.

[24] L. Puskar, E. Ritter, U. Schade, M. Yandrasits, S.J. Hamrock, M. Schaberg, E.F. Aziz, Infrared dynamics study of thermally treated perfluoroimide acid proton exchange membranes, Phys. Chem. Chem. Phys. 19 (2017) 626–635.

[25] B.R. Matos, E.I. Santiago, J.F.Q. Rey, C.H. Scuracchio, G.L. Mantovani, L.A. Hirano, F.C. Fonseca, Dc Proton conductivity at low-frequency in Nafion conductivity spectrum probed by time-resolved SAXS measurements and impedance spectroscopy, J. Polym. Sci., Part B: Polym. Phys. 53 (2015) 822.

[26] V. Felice, S. Ntais, A.C. Tavares, Propyl sulfonic acid functionalization of faujasite-type zeolites: effect on water and methanol sorption and on proton conductivity, Microporous Mesoporous Mater. 169 (2013) 128–136.

[27] S.A. Perusich, FTIR equivalent weight determination of perfluorosulfonate polymers, J. Appl. Polym. Sci. 120 (2011) 165–183.

[28] K.M. Cable, K.A. Mauritz, R.B. Moore, Effects of hydrophilic and hydrophobic counterions on the coulombic interactions in perfluorosulfonate Ionomers, J. Polym. Sci. B Polym. Phys. 33 (1995) 1065–1072.

[29] H. Kim, S. Prakash, W.E. Mustain1, P.A. Kohl, Sol–gel based sulfonic acid-functionalized silica proton conductive membrane, J. Power Sources 193 (2009) 562–569.

[30] Y. Zhou, R. Huang, F. Ding, A.D. Brittain, J. Liu, M. Zhang, M. Xiao, Y. Meng, L. Sun, Sulfonic acid-functionalized α-zirconium phosphate single-layer nanosheets as a strong solid acid for heterogeneous catalysis applications, ACS Appl. Mater. Interfaces 6 (2014) 7417–7425.

[31] K.A. Page, K.M. Cable, R.B. Moore, Molecular origins of the thermal transitions and dynamic mechanical relaxations in perfluorosulfonate ionomers, Macromolecules 38 (2005) 6472.

[32] A. Schönhals, F. Kremer, in: F. Kremer, A. Schönhals (Eds.), Broadband Dielectric Spectroscopy, Springer Verlag, Berlin, 2003, p. 59.

[33] B.R. Matos, J.S. da Silva, E.I. Santiago, D.F. Parra, D.J. Carastan, D.Z. de Florio, H. E. Andrada, A.C. Carreras, F.C. Fonseca, Proton and cesium conductivity in perfluorosulfonate ionomers at low and high relative humidity, Solid State Ionics 301 (2017) 86–94.